Simple Rotor Polarity Reversal Recovery in EV Traction Motor Sensorless Control

Myeong-Won Kim, and Jung-Wook Park
Yonsei University, South Korea

***Abstract*-- This paper presents a simple method to detect and recover rotor polarity reversal in sensorless traction motor control for electric vehicles (EVs). This rotor polarity reversal may happen during the sensorless control due to severe noise in the controller or the change in rotor position faster than bandwidth for position estimation. Although it can lead to the dangerous accident because torque is generated in the unintended direction, previous studies have lacked effective solutions to address this issue in real-time. The proposed method offers its prompt and reliable solution at any operating speed of traction motor. In addition, it is easy to implement and computationally efficient, making it suitable for accident prevention of EVs. Results from simulation and hardware-in-the-loop tests demonstrate the effectiveness of proposed method in recovering polarity reversal and improving the safety of EVs.**

***Index Terms*--automatic recovery method, electric vehicle, permanent magnet synchronous motor, polarity reversal, sensorless control**

I. Introduction

Recently, permanent magnet synchronous motors (PMSMs) have gained popularity as the traction motor in electric vehicles (EVs) due to their prominent efficiency and performance. Generally, PMSMs require the position sensor, such as an encoder or resolver, to accurately control. However, this increases the size and cost of drive system, as well as reduce its reliability due to mechanical vibration and noise. Thus, many sensorless control methods have been developed to drive PMSMs without the position sensor [1]–[15]. These methods can be categorized into two types based on the speed range of motor operation. For stationary and low speeds, signal-injection-based sensorless methods are mainly used [2]–[9], and back electromotive force (EMF)-based sensorless methods are applied for medium and high speeds [10]–[14]. To control traction motors in EVs across a wide range of speeds, both sensorless methods should be used, as shown in Fig. 1, where v_{abc}, i_{abc}, $v^{\hat{r}}_{dqs}$, $i^{\hat{r}}_{dqs}$, and $e^{\hat{r}}_{dqs}$ are the *a-b-c* phase voltages and currents, *d*- and *q*-axes voltages, currents, and extended back EMF components of estimated rotor reference frame, respectively. Also, $\hat{\theta}_r$, $\tilde{\theta}_r$, superscript $*$, subscript i are the estimated rotor position, position error, reference component, and the component of injected signal, respectively [15].

Meanwhile, when the controller is exposed to high levels of noise or when the rotor position is rapidly changed by external torque, the position estimation can be temporarily inaccurate during sensorless control due to limited bandwidth for position estimation. Although this

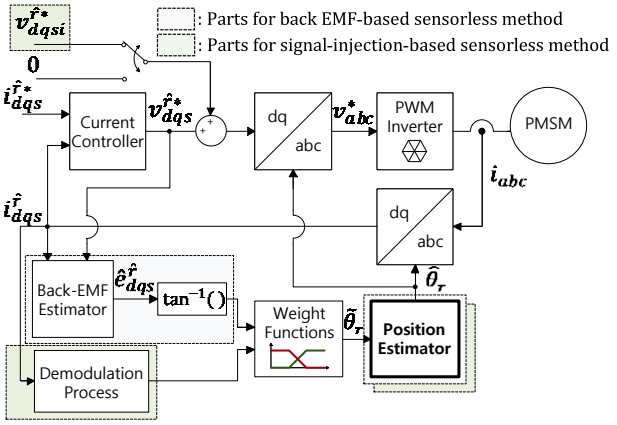

Fig. 1. Torque-speed characteristic of a three-phase induction motor.

usually stabilizes instantly, the polarity of $\hat{\theta}_r$ can be sometimes reversed in such situations, especially in the harsh environment of EVs. If the rotor polarity is reversed during the control, the output torque will be generated in the opposite direction, which can cause a dangerous accident while driving. In several restart methods, ways of detecting the rotor polarity have been introduced [16]–[18]. However, restarting the sensorless control at every unstable moment is not effective in this case because it takes a long time to restart the control, and polarity reversal does not occur at every unstable moment. Although a method of using the sign of back EMF was also proposed to detect the polarity reversal without restarting, it is still unreliable for low speeds [19].

In this paper, a simple method for solving the polarity reversal problem at all speed ranges of traction motor is proposed. The proposed method can effectively detect and recover polarity reversal during both sensorless controls with a simple algorithm. Therefore, it can protect the accident caused by polarity reversal in real-time. Its effectiveness is verified by hardware-in-the-loop tests in two representative sensorless methods.

II. Rotor Polarity Reversal in Traction Motor Sensorless Control

In sensorless methods, the rotor position information is usually extracted as $\tilde{\theta}_r$ from the relationship between voltage and current of traction motor drive system. In this relationship, $\tilde{\theta}_r$ is included in the trigonometric function. For example, a PWM switching frequency signal injection method [4] and extended back EMF method [8], which are representative signal injection-based and back EMF-based sensorless methods, respectively, have the following relationships, respectively:

$$\sin 2\tilde{\theta}_r = \frac{2L_{ds}L_{qs}}{(L_{ds}-L_{qs})\Delta T \cdot V_{inj}} \Delta i_{qsi}^{\hat{r}} \tag{1}$$

$$\tan \tilde{\theta}_r = -\frac{e_{ds}^{\hat{r}}}{e_{qs}^{\hat{r}}} \tag{2}$$

where L_{ds}, L_{qs}, ΔT, V_{inj}, and $i_{qsi}^{\hat{r}}$ are the stator inductances of d- and q-axes, half of switching period, amplitude of injected signal, and q-axis current variation caused by the injected signal of estimated rotor reference frame, respectively.

In practice, trigonometric operations place the high computational burden on the controller. For this reason, $\tilde{\theta}_r$ is often extracted in both sensorless methods by using a small-angle approximation, such as (3) and (4).

$$\tilde{\theta}_r \approx 0.5 \sin 2\tilde{\theta}_r \tag{3}$$

$$\tilde{\theta}_r \approx \tan \tilde{\theta}_r \,. \tag{4}$$

The extracted $\tilde{\theta}_r$ is used as the input of position estimator to estimate the rotor position. This position estimator has the specific bandwidth for position estimation while considering sensitivity of noise. It implies that the position estimator is vulnerable to unconsidered levels of noise and the rapid change in the rotor position may not be reflected in the position estimator. Thus, $\hat{\theta}_r$ is often momentarily inaccurate. To clarify its critical consequence, it is assumed that the rotor polarity is suddenly reversed and the incorrectly obtained position error, $\tilde{\theta}_r'$, is as different as π from $\tilde{\theta}_r$. Then, it should be noted that the rotor position information in (1) and (2) is unchanged with $\tilde{\theta}_r'$ as follows:

$$\sin 2\tilde{\theta}_r' = \sin 2(\tilde{\theta}_r + \pi) = \sin 2\tilde{\theta}_r \tag{5}$$

$$\tan \tilde{\theta}_r' = \tan(\tilde{\theta}_r + \pi) = \tan \tilde{\theta}_r \,. \tag{6}$$

That is, the position estimator still converges with $\tilde{\theta}_r'$, such that the control seems normal. The incorrectly estimated rotor reference frame has opposite directions for the d- and q-axes in comparison to the real rotor reference frame, as shown in Figs. 2(a) and (b). Accordingly, the current controls of motor drive system generate d- and q-axes currents with opposite directions. These currents generate the output torque in the opposite direction, which can compromise safety of EVs.

III. Proposed Recovery Method

A. Detection of Polarity Reversal

The stator voltage equation of PMSM is given as follows:

$$\begin{bmatrix} v_{ds}^r \\ v_{qs}^r \end{bmatrix} = \begin{bmatrix} R_s & \omega_r L_{qs} \\ \omega_r L_{ds} & R_s \end{bmatrix} \begin{bmatrix} i_{ds}^r \\ i_{qs}^r \end{bmatrix} + \begin{bmatrix} L_{ds} & 0 \\ 0 & L_{qs} \end{bmatrix} \frac{d}{dt} \begin{bmatrix} i_{ds}^r \\ i_{qs}^r \end{bmatrix} + \begin{bmatrix} 0 \\ \omega_r \lambda_f \end{bmatrix} \tag{7}$$

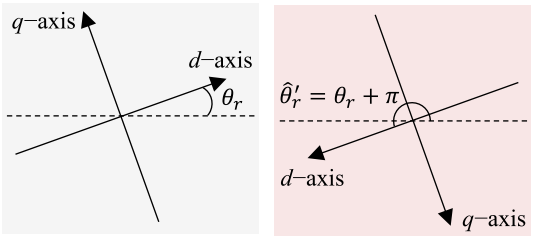

(a) (b)

Fig. 2. (a) Real rotor reference frame. (b) Incorrectly estimated rotor reference frame.

where v_{dqs}^r, i_{dqs}^r, ω_r, and λ_f are d- and q-axes voltages, currents of real rotor reference frame, and rotor speed, and linkage magnetic flux, respectively. When the rotor polarity is reversed, the signs of voltage and current terms of (7) become negative because directions of d- and q-axes in the estimated rotor reference frame are opposite to those in the real rotor reference frame. Then the back EMF is obtained in the controller as follows:

$$\hat{v}_{bemf} = v_{qs}^{\hat{r}*} - \hat{R}_s i_{qs}^{\hat{r}} - \hat{\omega}_r \hat{L}_{qs} i_{qs}^{\hat{r}} - \hat{L}_{ds} \frac{d}{dt} i_{ds}^{\hat{r}} \tag{8}$$

where $\hat{v}_{bemf}$ mean the calculated back EMF. It becomes different sign in this situation due to the reversed signs of voltage and current. Whereas the sign of real back EMF, $v_{bemf} = \omega_r \cdot \lambda_f$, is not changed in (7) because ω_r and λ_f can be treated as constants. For this reason, the sign of $\hat{v}_{bemf}$ seems to have the opposite to the sign of ω_r. Thus, rotor polarity reversal can be easily detected by comparing the signs of $\hat{v}_{bemf}$ and $\hat{\omega}_r$ during the back EMF-based sensorless control, where $\hat{\omega}_r$ mean the estimated speed. In other words, the polarity is reversed if $\hat{v}_{bemf} \cdot \hat{\omega}_r < 0$. However, some filters and position estimator in the sensorless control cause the delay, which also delays the calculation of $\hat{v}_{bemf}$. Accordingly, to further ensure this result, the time to converge $\tilde{\theta}_r$ to zero, τ_{cvg}, should be needed as part of preventing malfunction.

During the signal-injection-based sensorless control, it is difficult to detect polarity reversal with v_{bemf} because it is small at low speeds. Therefore, in this case, the rotor polarity is identified based on the magnetic saturation of stator core. Due to this, the actual value of inductance changes depending on the current, as shown in Fig. 3. When the rotor polarity is normal, i.e., when the positive d-axis is in the N-pole direction, the positive voltage of $v_{dsi}^{\hat{r}}$ excites the saturation of stator core and reduces L_{ds}. It means that the d-axis current variation caused by the injected signal, $\Delta i_{dsi}^{\hat{r}}$, is larger than the ideal value calculated with the nominal L_{ds}. Conversely, when the rotor polarity is revered, $\Delta i_{dsi}^{\hat{r}}$ is smaller than ideal value. In the proposed method, the average $\Delta i_{dsi}^{\hat{r}}$ is measured for the certain time, τ_{avg}, while maintaining the reference current value for the current control and injecting the signal. Thereafter, the inverted signal is injected for the same time of τ_{avg} to obtain the average $\Delta i_{dsi}^{\hat{r}}$ during this time. Then, as shown in Fig. 4, if the first measured average $\Delta i_{dsi}^{\hat{r}}$ is smaller than the second measured average $\Delta i_{dsi}^{\hat{r}}$, it can be determined that the rotor polarity

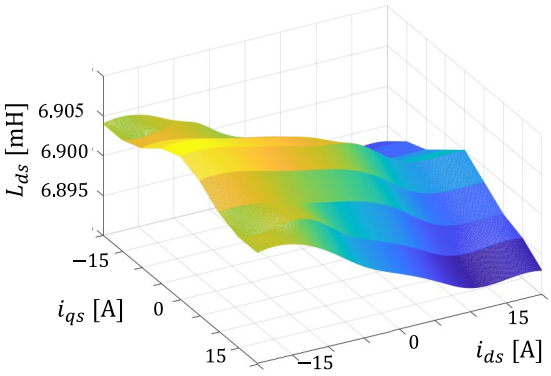

Fig. 3. *d*-axis inductance according to currents.

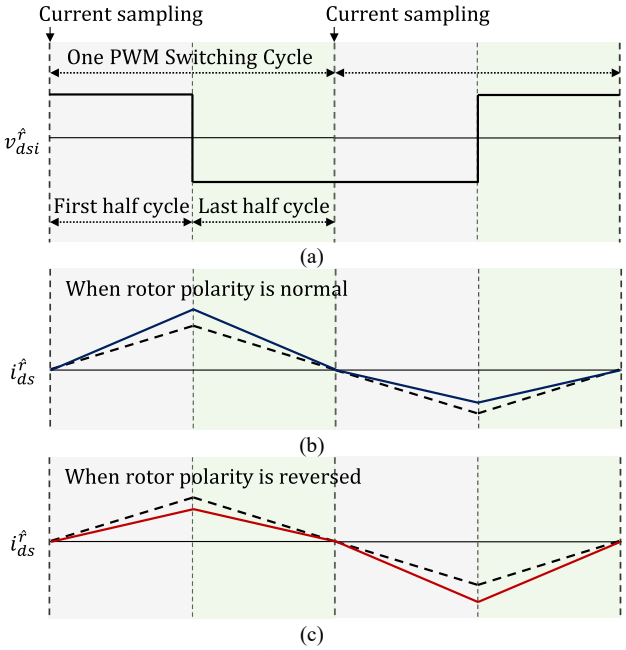

Fig. 4. Waveforms of (a) injected *d*-axis voltage, (b) *d*-axis current without polarity reversal, and (c) *d*-axis current with polarity reversal.

is reversed. Likewise, this sequence requires τ_{cvg} because this sequence must be under the assumption that the *d*-axis is aligned with the rotor. Also, if the measurement error is severe, τ_{avg} or the amplitude of signals for identifying the rotor polarity should be increased for the reliability.

B. Implementation of Recovery Algorithm

The detection of polarity reversal is executed in the proposed method when the magnitude of $\tilde{\theta}_r$ is larger than 0.8 because the rotor polarity may be reversed at this moment. If polarity reversal is detected by detection methods, the signal for confirming the reversed polarity, S_{rev}, is generated. Then $\hat{\theta}_r$ is compensated by π for recovery. Subsequently, S_{rev} is cleared, and the algorithm is repeated after the holding time, τ_{hld}, to avoid responding to $\tilde{\theta}_r$ fluctuated by the compensation. The overall algorithm of proposed method is shown in Fig. 5, where the average $\Delta i_{dsi1}^{\hat{r}}$ and average $\Delta i_{dsi2}^{\hat{r}}$ are the first and second measured average $\Delta i_{dsi}^{\hat{r}}$, respectively.

The proposed method is basically for when the position estimation in sensorless control is momentarily unstable and then converges again. Therefore, it cannot

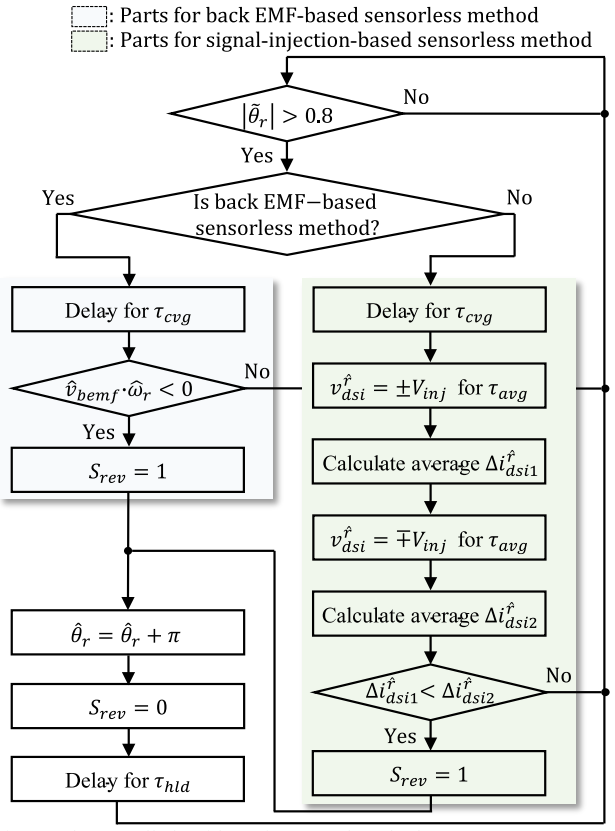

Fig. 5. The overall algorithm of proposed method.

solve the complete failure of sensorless control, which cannot continuously estimate the position. Instead, in this case, the controller should be turned off and restarted by existing flying start methods [20], [21]. In other words, this algorithm when the position error does not converge should also be used along with the proposed method to ensure the stability of sensorless control in actual EVs although it is not specifically described in this paper.

C. Improvement of Recovery Speed Performance

After instantaneous instability of control due to sudden disturbances, τ_{cvg} is dependent on the performance of position estimator in both sensorless control methods. Considering this aspect, it is important to appropriately select τ_{cvg} for the proposed method. Nevertheless, when the total delay time becomes excessively long due to noise in the traction motor drive system, the practical effectiveness of proposed method can be compromised. To prevent this, the proposed method can utilize some properties of conventional sensorless methods to optimize delay times and effectively contribute to the safety of EVs in various speed ranges.

In the back EMF-based method, v_{bemf} is proportional to ω_r. Consequently, when exposed to the same noise level, the signal-to-noise ratio of $\hat{v}_{bemf}$ tends to be higher at high speeds, thereby enhancing reliability of detection result Therefore, in the proposed method, the total delay time can be minimized by setting τ_{cvg} short at high speed and utilizing the signal injection-based method within the medium speed range that excessive total delay time.

Similarly, in the signal injection-based method, the

large magnitude of V_{inj} leads to the large magnitude of $\Delta i_{dsi}^{\hat{r}}$. It means that the signal-to-noise ratio of $\Delta i_{dsi}^{\hat{r}}$ becomes relatively larger with the larger injected signal. Thus, by amplifying V_{inj} for identifying rotor polarity, τ_{avg} can be reduced, and the total delay time can be ultimately reduced.

IV. Experimental Verification

The proposed method was evaluated by the hardware-in-the-loop tests to validate its effectiveness. The setup for hardware-in-the-loop consisted of a real-time digital simulator (RTDS), which was utilized to create the PMSM and load environment. Accordingly, the polarity reversal situation was safely implemented without excessive real hardware manipulation. To establish the PMSM drive system parameters listed in Table I and operate the load, the design program on the PC was used. The system model considers the inductance saturation in Fig. 3. Additionally, a digital signal processor (DSP) was connected to the RTDS to facilitate the implementation of the drive system, including sensorless control. Furthermore, the proposed method was incorporated into the DSP system. The configurations of these setups can be observed in Fig. 6.

A. Polarity Reversal Recovery with Back EMF-Based Sensorless Control

While the PMSM is controlled by the back EMF-based sensorless control at the speed of 1440 rpm, polarity reversal occurs, as shown in Fig. 7. It can be observed that the position error is momentarily fluctuated by sudden disturbances. However, it converges to zero in the highly short time even though the polarity is reversed. As the result, the sign of $\hat{v}_{bemf}$ is also reversed. As described for the proposed method in Section III-A, polarity reversal is detected after τ_{cvg} of 0.07 s because the initial calculated result of $\hat{v}_{bemf}$ is not accurate after polarity reversal. Then S_{rev} is generated, and the polarity is recovered.

In contrast, when the polarity is not reversed after the sensorless control becomes unstable instantaneously, implementation of proposed method is shown in Fig. 8. Because the sign of back EMF does not change even after 0.07 seconds, S_{rev} is not generated. As the result, the polarity remains the same.

B. Polarity Reversal Recovery with Signal-Injection-Based Sensorless Control

When the PMSM is driven by the signal-injection-based sensorless control at the speed of 10 rpm, recovery results are shown in Fig. 9. For the proposed method, the amplitude of signals for identifying the rotor polarity is set to twice V_{inj}, i.e., 40 V, and τ_{avg} is set to 0.05 s. The algorithm waits until $\tilde{\theta}_r$ converges to zero during τ_{cvg} of 0.1 s after reversing the rotor polarity. Thereafter, polarity reversal is determined with the generation of S_{rev} after two τ_{avg}, thereby compensating $\hat{\theta}_r$ by π. It should be noted that this time is short enough to prevent the serious accident.

The case when no polarity reversal occurs is shown in

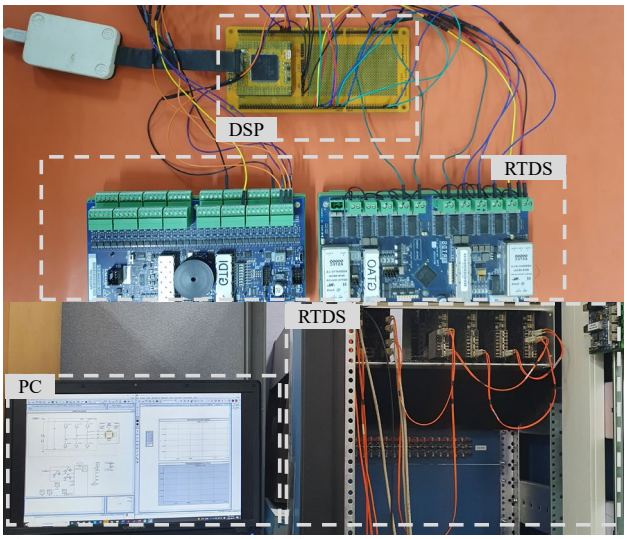

Fig. 6. Setup for hardware-in-the-loop test.

TABLE I
Parameters of PMSM Drive System

Parameter	Symbol	Value
DC-link voltage	V_{DC}	400 V
PWM Switching frequency	f_{sw}	5 kHz
Rated torque	T_{rated}	320 N·m
Rated Power	P_{rated}	180 kW
Stator Resistance	R_s	0.719 Ω
Stator inductance	L_{ds}/L_{qs}	6.9/9.8 mH
Linkage magnetic flux	λ_f	0.41 Wb

Fig. 10. After $\tilde{\theta}_r$ fluctuations, polarity reversal is judged according to the procedure of proposed method. However, because the polarity is not reversed, S_{rev} is not made, and the polarity does not change. Consequently, it is verified that polarity reversal is promptly detected and recovered with reliability by the proposed method in all sensorless controls.

V. Conclusions

This paper proposes a method for preventing the potentially dangerous consequences of rotor polarity reversal during the sensorless traction motor control in electric vehicles (EVs). It can be used at all speed range of traction motor because it deals with both signal-injection-based and back electromotive force-based sensorless methods. The results of hardware-in-the-loop tests show that the proposed method reliably and quickly recovers polarity reversal in a short time after detecting it. Ultimately, the proposed method can provide a practical and effective assistance to implement the traction motor sensorless control for EVs.

Acknowledgment

This work was supported by the National Research Foundation of Korea (NRF) grant funded by the Ministry of Science and ICT (MIST), Korea government (No. 2020R1A3B2079407).

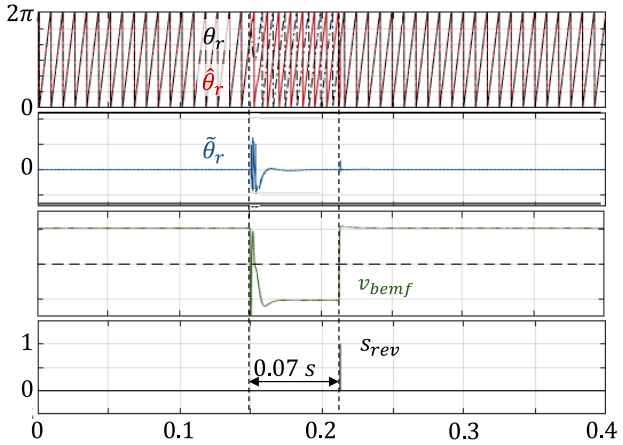

Fig. 7. Real position, estimated position, position error, injected *d*-axis voltage, and polarity reversal signal when the polarity is reversed during the back EMF-based sensorless control.

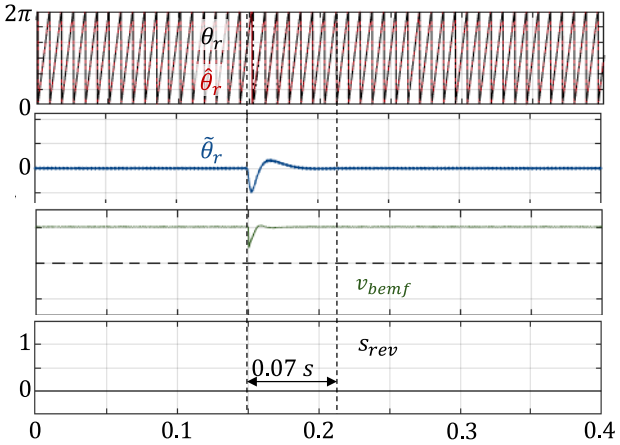

Fig. 8. Real position, estimated position, position error, injected *d*-axis voltage, and polarity reversal signal when the polarity is not reversed during the back EMF-based sensorless control.

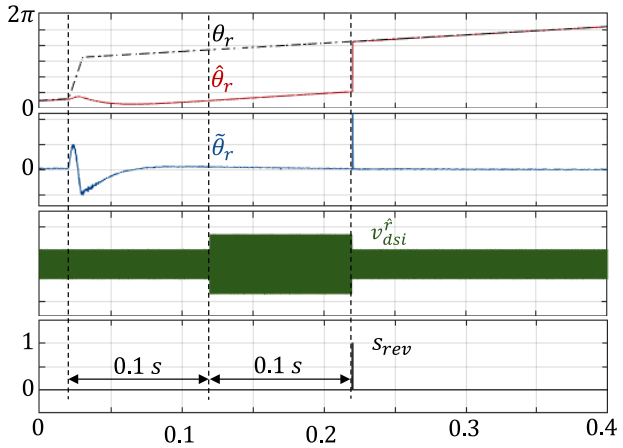

Fig. 9. Real position, estimated position, position error, injected *d*-axis voltage, and polarity reversal signal when the polarity is reversed during the signal-injection-based sensorless control.

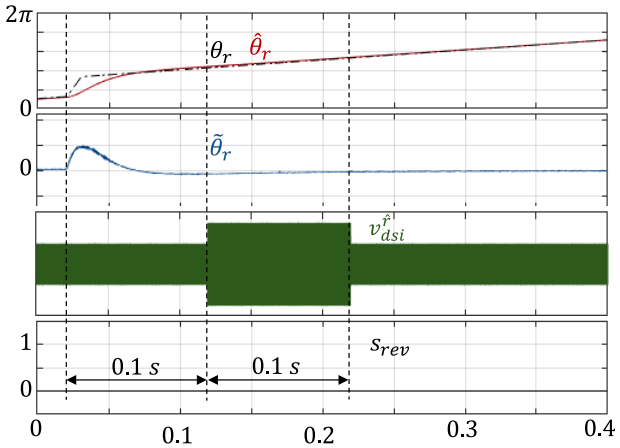

Fig. 10. Real position, estimated position, position error, injected *d*-axis voltage, and polarity reversal signal when the polarity is not reversed during the signal-injection-based sensorless control.

REFERENCES

[1] Y. Li, H. Wu, X. Xu, X. Sun, and J. Zhao, "Rotor position estimation approaches for sensorless control of permanent magnet traction motor in electric vehicles: a review," *World Electric Vehicle Journal*, vol. 12, no. 1, p. 9, 10-Jan. 2021.

[2] J.-I. Ha and S.-K. Sul, "Sensorless field-orientation control of an induction machine by high-frequency signal injection," *IEEE Trans. Ind. Appl.*, vol. 35, no. 1, pp. 45–51, Jan./Feb. 1999.

[3] Y.-D. Yoon, S.-K. Sul, S. Morimoto, and K. Ide, "High-bandwidth sensorless algorithm for AC machines based on square-wave-type voltage injection," *IEEE Trans. Ind. Appl.*, vol. 47, no. 3, pp. 1361-1370, May/Jun. 2011.

[4] S. Kim, J.-I. Ha, and S.-K. Sul, "PWM switching frequency signal injection sensorless method in IPMSM," *IEEE Trans. Ind. Appl.*, vol. 48, no. 5, pp. 1576–1587, Sep./Oct. 2012.

[5] F. Briz, M. W. Degner, P. Garcia, and R. D. Lorenz, "Comparison of saliency-based sensorless control techniques for AC machines," *IEEE Trans. Ind. Appl.*, vol. 40, no. 4, pp. 1107–1115, Jul./Aug. 2004.

[6] Z. Lin, X. Li, Z. Wang, T. Shi, and C. Xia, "Minimization of additional high-frequency torque ripple for square-wave voltage injection IPMSM sensorless drives," *IEEE Trans. Power Electron.*, vol. 35, no. 12, pp. 13345–13355, Dec. 2020.

[7] G. Wang, L. Yang, G. Zhang, X. Zhang, and D. Xu, "Comparative investigation of pseudorandom high-frequency signal injection schemes for sensorless IPMSM drives," *IEEE Trans. Power Electron.*, vol. 32, no. 3, pp. 2123–2132, Mar. 2017.

[8] G. Zhang, G. Wang, H. Wang, D. Xiao, L. Li, and D. G. Xu, "Pseudorandom-frequency sinusoidal injection based sensorless IPMSM drives with tolerance for system delays," *IEEE Trans. Power Electron.*, vol. 34, no. 4, pp. 1–10, Apr. 2018.

[9] G. Zhang et al., "Pseudorandom-frequency sinusoidal injection for position sensorless IPMSM drives considering sample and hold effect," *IEEE Trans. Power Electron.*, vol. 34, no. 10, pp. 9929–9941, Oct. 2019.

[10] N. Matsui, "Sensorless PM brushless DC motor drives," *IEEE Trans. Ind. Appl.*, vol. 43, no. 2, pp. 300-308, Apr. 1996.

[11] B.-H. Bae, S.-K. Sul, J.-H. Kwon, and J.-S. Byeon, "Implementation of sensorless vector control for superhigh-speed PMSM of turbo-compressor," *IEEE Trans. Ind. Appl.*, vol. 39, no. 2, pp. 811-818, May/Jun. 2003.

[12] S. Morimoto, K. Kawamoto, M. Sanada, and Y. Takeda, "Sensorless control strategy for salient-pole PMSM based on extended EMF in rotating reference frame," *IEEE Trans. Ind. Appl.*, vol. 38, no. 4, pp. 1054-1061, Jul./Aug. 2002.

[13] Z. Chen, M. Tomita, S. Doki, and S. Okuma, "An extended electromotive force model for sensorless control of interior permanent-magnet synchronous motors," *IEEE Trans. Ind. Electron.*, vol. 50, no. 2, pp. 288-295, Apr. 2003.
[14] A. B. Kulkarni and M. Ehsani, "A novel position sensor elimination technique for the interior permanent-magnet synchronous motor drive," *IEEE Trans. Ind. Appl.*, vol. 28, no. 1, pp. 144–170, Jan./Feb. 1992.
[15] Z. Ma, J. Gao, and R. Kennel, "FPGA implementation of a hybrid sensorless control of SMPMSM in the whole speed range," *IEEE Trans. Ind. Inf.*, vol. 9, no. 3, pp. 1253–1261, Aug. 2013.
[16] X. Zhang, H. Li, S. Yang, and M. Ma, "Improved Initial Rotor Position Estimation for PMSM Drives Based on HF Pulsating Voltage Signal Injection," *IEEE Trans. Ind. Electron.*, vol. 65, no. 6, pp. 4702–4713, Jun. 2018.
[17] I. Szalay, D. Fodor, K. Enisz, and H. Medve, "Permanent Magnet Synchronous Motor Model Extension for High-Frequency Signal Injection-Based Sensorless Magnet Polarity Detection," *Energies*, vol. 15, no. 3., pp. 1131–1155, Feb. 2022.
[18] G. Bi, G. Wang, G. Zhang, N. Zhao, and D. Xu, "Low-Noise Initial Position Detection Method for Sensorless Permanent Magnet Synchronous Motor Drives," *IEEE Trans. on Power Electron.*, vol.35, no. 12, pp.13333–13344, Dec. 2020.
[19] M.-W. Kim, I. Kim, and J.-W. Park, "Automatic Recovery Method for Reversal of Rotor Polarity in Traction Motor Sensorless Control for Electric Vehicles," in *Proc. 2022 IEEE Energy Conv. Cong. and Expo.*, 2022.
[20] S. Taniguchi, S. Mochiduki, T. Yamakawa, S. Wakao, K. Kondo, and T. Yoneyama, "Starting Procedure of Rotational Sensorless PMSM in the Rotating Condition," *IEEE Trans. Ind. Appl.*, vol.45, no. 1, pp.194–202, 2009.
[21] K. Lee, S. Ahmed, and S. M. Lukic, "Universal Restart Strategy for High-Inertia Scalar-Controlled PMSM Drives," *IEEE Trans. Ind. Appl.*, vol.52, no. 5, pp.4001–4009, Sep-2016.